Magnetic properties of $Bi_{0.75}Sr_{0.25}MnO_3$ ($x \approx 2/8, T_{CO}=600$ K): Ferromagnetism and charge order

José Luis García-Muñoz,[1] Carlos Frontera,[1] Marc Respaud,[2] Maud Giot,[3] Clemens Ritter,[4] and Xavier G. Capdevila[5]
[1]*Institut de Ciència de Materials de Barcelona, CSIC, Campus Universitari de Bellaterra, E-08193 Bellaterra, Spain*
[2]*Laboratoire de la Physique de la Matière Condensée, INSA, F-31077 Toulouse Cedex-4, France*
[3]*Laboratoire CRISMAT, UMR CNRS/ISMRA, 6 Boulevard du Maréchal Juin, F-14050 Caen Cedex, France*
[4]*Institut Laue Langevin, Boîte Postale 156, F-38042 Grenoble Cedex 9, France*
[5]*Departameto d'Enginyeria Química i Metal. lúrgia, Universitat de Barcelona, Facultat de Química, E-08028 Barcelona, Spain*
(Received 6 April 2005; revised manuscript received 8 June 2005; published 22 August 2005)

The possible coexistence of ferromagnetism and charge/orbital order in $Bi_{3/4}Sr_{1/4}MnO_3$ has been investigated. The manganite $Bi_{0.75}Sr_{0.25}MnO_3$, with commensurate charge balance, undergoes an electronic transition at $T_{CO} \sim 600$ K that produces a long-range modulation with double periodicity along the *a* and *c* axes, and unusual anisotropic evolution of the lattice parameters. The magnetic properties of this new ordered phase were studied by neutron powder diffraction and high-magnetic fields. In zero field the magnetic structure is globally antiferromagnetic, ruling out the apparition of spontaneous ferromagnetism. However, the application of magnetic fields produces a continuous progressive canting of the moments, inducing a ferromagnetic phase even for relatively small fields ($H \ll 1$ T). Application of pulsed high fields produces a remarkable and reversible spin polarization (under 30 T, the ferromagnetic moment is $\sim 3\ \mu_B$/Mn, without any sign of charge order melting). The coexistence of ferromagnetism and charge order at low and very-high fields is a remarkable property of this system.

DOI: 10.1103/PhysRevB.72.054432 PACS number(s): 71.30.+h, 71.38.−k, 71.45.Lr, 75.25.+z

I. INTRODUCTION

In mixed-valence metal oxides the electronic-type transitions related with charge localization, orbital ordering (OO) assisted by the Jahn-Teller effect, and charge ordering (CO) are currently the object of intense investigations.[1–8] Recently, the Bi−Sr−Mn−O system has received great attention due to the observation of some singularities that differ from the general behavior of previously studied manganites.[9–16] One is the great tendency of Bi−Sr manganites to present charge-order (CO) at very high temperatures.[9,10] Another one is the presence in the electron microscopy images at atomic resolution of internal periodic structures consistent with double stripes of MnO_6 octahedra,[11,14] which still do not have a convincing justification. The study of this family is of importance in the context of the search for a satisfactory physical description of the ground state of modulated manganites. Different scenarios have been proposed describing the electronic configuration of checkerboard and stripe phases in these oxides: real space ordering of ionic species (Mn^{3+}, Mn^{4+}),[3–7,17] charge density waves ($Mn^{3.5-\delta}$, $Mn^{3.5+\delta}$) or continuous valence fluctuations,[18–20] charge localization in nanometric areas involving more than one atom ($Mn^{3.5}$, Zener polarons),[8,17] etc.

In Refs. 9 and 10 we reported a spectacularly high orbital/charge ordering temperature ($T_{CO}=525$ K) in $Bi_{0.50}Sr_{0.50}MnO_3$, approximately 200 K above the ordering temperature in $Bi_{0.50}Ca_{0.50}MnO_3$. Although an accurate determination of the atomic displacements is still pending and will require meticulous single crystal studies, analysis of the weak superlattice peaks in the powder diffraction patterns signaled a subtle modulation of the same type as the CO phase in lanthanide based $Ln_{0.50}Ca_{0.50}MnO_3$ compounds. The magnetic structure in $Bi_{0.50}Sr_{0.50}MnO_3$ was also consistent with this analogy: a CE-type antiferromagnetic ordering of manganese moments was reported in Ref. 10. It has been inferred that a likely hybridization of 6*s*-Bi orbitals with 2*p*-O orbitals can be at the origin of the new mechanism favoring charge order in this family of oxides. Curiously, the unpredicted mechanism is much less active in more distorted Bi−Ca perovskites than in Bi−Sr manganites.[9,10,15] From high-resolution electron microscopy studies,[11] a contrast modulation characterized by alternating double rows of MnO_6 octahedra parallel to the Mn layers is a distinctive feature (not yet well elucidated) of highly stable charge-order phases in Bi−Sr−Mn−O compounds. Such contrast has been observed in the images of distinct charge-order phases (as the ordered phases with doping $x=1/3$ and $1/2$).[11,14]

Moreover, the dependence of the properties of $Bi_{1-x}Sr_xMnO_3$ compounds on the Bi content is, up to a great extent, still an open issue. The composition $Bi_{0.75}Sr_{0.25}MnO_3$ is particularly appealing due to its commensurability ($x=1/4=1/8+1/8$). With this particularity in mind (compatibility with integer period modulations), we performed a high-temperature neutron and synchrotron powder diffraction study[13,16] revealing that $Bi_{0.75}Sr_{0.25}MnO_3$ undergoes a charge-order transition at $T_{CO}=600$ K, well above the ordering temperature in half doped $Bi_{0.5}Sr_{0.5}MnO_3$ ($T_{CO}=525$ K). A structural study of $Bi_{3/4}Sr_{1/4}MnO_3$ between room temperature (RT) and 750 K was reported Ref. 16. The existence of a new type of charge-ordered phase in this compound was concluded from the stabilization of a commensurate modulation and the appearance of weak superstructure reflections different from the characteristic lines previously observed in other modulated manganites. So, RT electron diffraction patterns showed the presence of a new type of

superstructure, common to the compositions $Bi_{0.67}Sr_{0.33}MnO_3$ (Ref. 14) and $Bi_{0.75}Sr_{0.25}MnO_3$ (Ref. 16). The superstructure doubles two of the pristine cell parameters, instead of the usual one in CO manganites. This double modulation has also been confirmed in $Bi_{1-x}Sr_xMnO_3$ (for $x \sim 0.25-0.33$) by means of the superstructure peaks observed in neutron and synchrotron powder diffraction patterns. Although the samples studied were single phased and the number of superstructure reflections detected was high, these were not enough to refine the superstructure and only an average structure could be determined.[16] The superstructure signaling a new type of modulated phase was found to disappear above $T_{CO} \sim 600$ K. Concomitant with this, the average structure changes from *Ibmm* (below T_{CO}) to *Pbnm* (above T_{CO}).[16] The symmetry change in this transformation is also very intriguing and different from the usual behavior in modulated manganites, where the low temperature structure is simply a modulation of the high temperature structure. A substantial enlargement of the *a* parameter accompanies this structural transition, while *b* and *c* shrink on cooling through T_{CO}.[16] Hence this lattice evolution is also different from the usual enlargement of *a* and *b* and the shrink of *c* lattice parameters found in half doped or underdoped manganites.[3–9] The observation of these structural features led us to conclude that an ordered localization of e_g electrons takes place around 600 K, but the structural changes and lattice evolution are very different to the changes observed in $Bi_{1/2}Sr_{1/2}MnO_3$. This strongly indicates that a different charge-order phase occurs for the commensurate charge balance of $Bi_{3/4}Sr_{1/4}MnO_3$.

In this paper we have extended our previous investigations (centered in the high temperature range) to the interval of low temperatures, studying the magnetic and structural properties of the system $Bi_{3/4}Sr_{1/4}MnO_3$ below RT.

II. EXPERIMENTAL DETAILS

Polycrystalline $Bi_{0.75}Sr_{0.25}MnO_3$ ceramics were prepared following a sol-gel route, starting from stoichiometric quantities of Bi_2O_3 (99.9%), MnO_2 (99.99%), and $SrCO_3$ (99.99%). They were dissolved in concentrated nitric acid, the solution jellified according to the acrylamide polymerization method,[21] and then subjected to self-ignition. The corresponding powders were heated at 700 °C for 12 h and then to 950 °C for 12 h in flowing oxygen. Sol-gel synthesis was chosen with the purpose of obtaining a single-phase material and to minimize a possible Bi deficiency due to evaporation. The samples for transmission electron microscopy were prepared by smoothly crushing the crystals in alcohol. The small flakes were deposited on a holey carbon film supported by a copper grid. The electron diffraction (ED) study was carried out using a JEOL 200 CX microscope fitted with a eucentric goniometer (±60°) and equipped with an energy dispersive spectroscopy (EDS) analyzer. Tilting around the crystallographic axes was carried out for reconstructing the reciprocal space.

Neutron powder diffraction (NPD) patterns were collected at the Institut Laue-Langevin (Grenoble, France) in the temperature interval $1.5 < T < 750$ K. Several diffractometers and wavelengths were used: high resolution D2B ($\lambda = 1.594$ Å, in its high flux mode) and D1B ($\lambda = 2.52$ Å). Synchrotron x-ray powder diffraction (SXRPD) patterns were collected on BM16 ($\lambda = 0.540092$ Å) diffractometer of ESRF (Grenoble, France). The x-ray absorption by bismuth atoms was minimized by mixing the sample with diamond powder and using a thin borosilicate glass capillary of $\phi = 0.3$ mm. The Rietveld method and FULLPROF program[22] were used for diffraction data analysis. Susceptibility was measured over the range $5 < T < 700$ K. Magnetic measurements were done using a superconducting quantum interference device (SQUID) magnetometer. Magnetotransport characterization was performed by the four-probe method, using a commercial PPMS system (Quantum Design) in the temperature range $5 < T < 350$ K. High-magnetic-field M(H) curves were measured at the facilities of the LNCMP in Toulouse (France).

III. RESULTS AND DISCUSSION

A. Electron microscopy

The combined electron diffraction (ED)/cationic analysis (EDS) characterization of the powder used in this study was carried out on about 50 grains. The sample exhibits a very good crystallinity and the average composition (calculated for one Mn per formula unit) is close to $Bi_{0.71\pm0.04}Sr_{0.29\pm0.04}Mn$, in the limit of accuracy of the technique (nominally $Bi_{0.75}Sr_{0.25}MnO_3$). A second observation of the electron microscopy study concerns the habits of the grains. In the title sample, the grains are faceted and their average size is of the order of the micrometer [Fig. 1(a)]. A different habit is commonly observed for other compositions obtained from the same sol-gel synthesis process, as, for example, $x = 0.50$ and 0.55 (Ref. 24) (small spherical crystallites, forming large tunnels and having an average diameter of the order of a few tens of nanometers). At room temperature, the reconstruction of the reciprocal space showed that a large majority (more than 90%) of the crystals exhibit a superstructure with regard to the classical distorted perovskite cell, namely $a_p\sqrt{2} \times a_p\sqrt{2} \times 2a_p$ (a_p is for the ideal cubic perovskite). It is the same superstructure as the previously reported one for $Bi_{2/3}Sr_{1/3}MnO_3$, and can be described by the appearance of a double modulation, $1/2a^*$ and $1/2c^*$, referred to as the *Ibmm*-type subcell. The [001] ED pattern is given in Fig. 1(b), indexed in the *Ibmm* subcell setting; the satellites along a^* are indicated with white arrows. The extra reflections generated by the modulation along c^* are clearly visible in the $[2\bar{1}0]$ ED patterns, as shown in Fig. 1(c) (see the white triangles). Hence these observations agree with the superstructure reported in Refs. 14 and 16: an orthorhombic supercell, with a *P*-type space group and the doubling of the ***a*** and ***c*** parameters ($2a_p\sqrt{2} \times a_p\sqrt{2} \times 4a_p$). The crystallites of the minority phase (about 5%) are characterized by the absence of extra reflections, i.e., they exhibit the reflections of the *Ibmm* subcell. The corresponding EDS analysis evidenced a small but significant Mn deficiency with regard to the ideal perovskite composition. Small traces ($\sim 1\%$) of Mn_3O_4 were also detected.

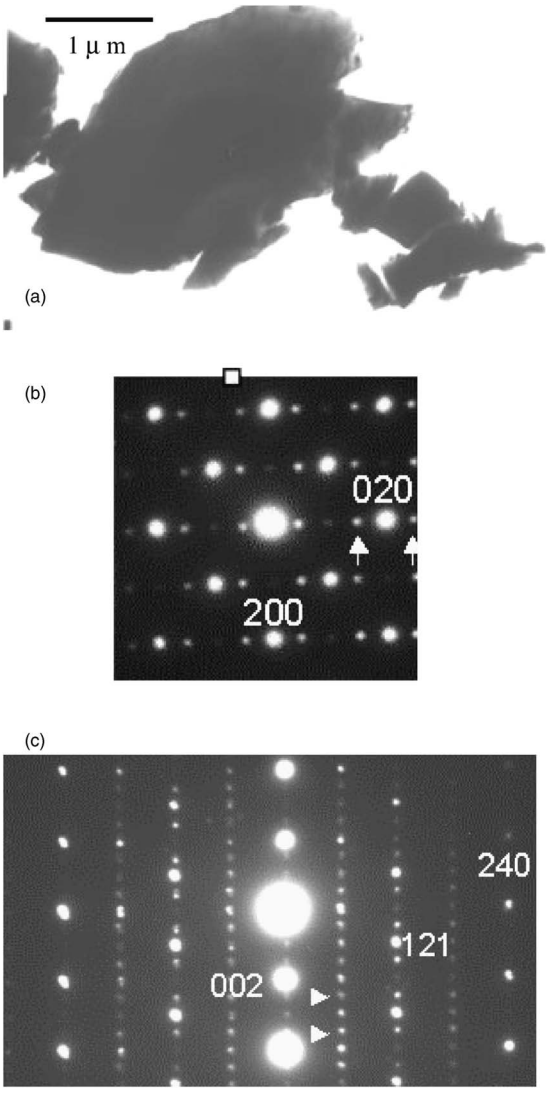

FIG. 1. (a) Overall bright field image of $Bi_{0.75}Sr_{0.25}MnO_3$ prepared by sol-gel. (b) [001] ED patterns recorded at RT (referred to as the *Ibmm* subcell). Arrows signal the satellites in commensurate positions corresponding to the modulation along a^*. (c) $[2\bar{1}0]$ ED patterns showing the extra spots from the new periodicity along the *c* axis.

B. Magnetic and magnetotransport measurements

The inverse dc magnetic susceptibility of $Bi_{0.75}Sr_{0.25}MnO_3$ is shown in Fig. 2 between 5 and 700 K. Two well-separated transitions are observed. The first one, at high temperature [Fig. 2(a)] signals the charge-order transition at $T_{CO} \sim 600$ K, reported in Ref. 16. As happens in $Bi_{0.50}Sr_{0.50}MnO_3$, the charge-order transition is accompanied by a considerable enhancement (on cooling) of the paramagnetic effective moment of Mn ions. Above T_{CO}, the effective moment is $\mu_{eff}[\text{exp}]=4.68(4)\ \mu_B/\text{Mn}$. The Curie-Weiss behavior in the paramagnetic region below T_{CO} corresponds to $\mu_{eff}=5.26(2)\ \mu_B/\text{Mn}$ and $\theta_c=+104(2)K$ ($120\ \text{K} < T < 575\ \text{K}$). We note that the effective moment found below T_{CO} does not agree with the ordering of ionic Mn^{3+} and Mn^{4+} species, as discussed in Ref. 16. The second

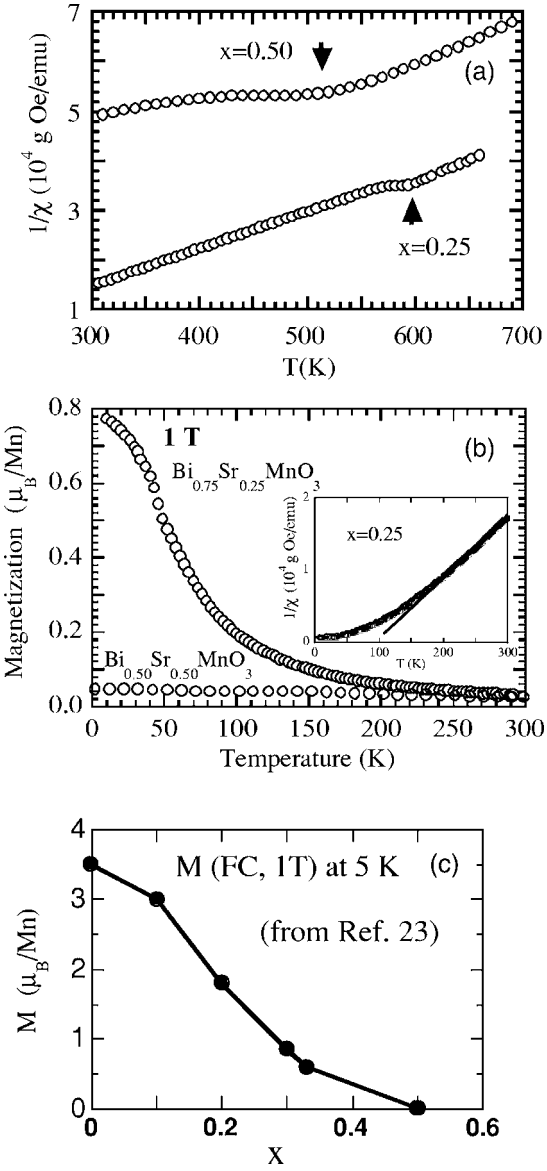

FIG. 2. (a) Inverse susceptibility showing the CO transition in $Bi_{1-x}Sr_xMnO_3$ $x=0.25$ and 0.50 oxides (H=1 T, curves have been shifted for the sake of clarity). (b) Comparison of the temperature dependence of the magnetization of $Bi_{0.75}Sr_{0.25}MnO_3$ and $Bi_{0.50}Sr_{0.50}MnO_3$ measured in 1 T (FC) below RT. Inset: inverse susceptibility. (c) M(1 T,5 K) vs *x* by Chiba *et al.* (data from Ref. 23).

transition observed in Fig. 2 corresponds to the onset of magnetic ordering below ≈120 K. Figure 2(b) suggests a magnetic transition from paramagnetic to a ferro or ferrimagnetic phase (note that these measurements were performed under 1 T of applied field).

The resistivity below room temperature of $Bi_{0.75}Sr_{0.25}MnO_3$ in zero field and 5 T is shown in Fig. 3. In the same figure the resistivity of $Bi_{0.5}Sr_{0.5}MnO_3$ is also shown for comparison. The resistivity of both polycrystalline samples is relatively high, and values for $x=1/4$ are not very different to those of the $x=1/2$ composition. According to the high T_{CO}'s values in Bi–Sr perovskites, there are no jumps in the resistivity below ambient temperature, where

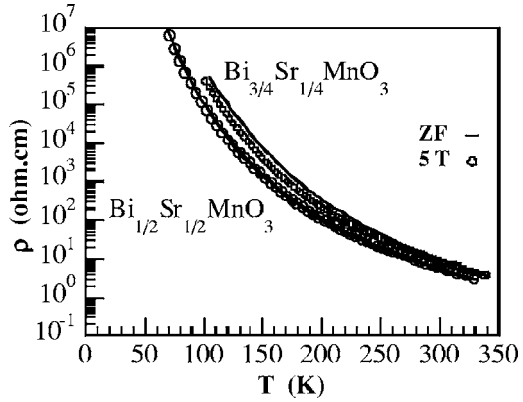

FIG. 3. Comparison of the electrical resistivity of $Bi_{3/4}Sr_{1/4}MnO_3$ and $Bi_{1/2}Sr_{1/2}MnO_3$, in zero field (continuous line) and under a field of 5 T (circles).

$Bi_{0.75}Sr_{0.25}MnO_3$ presents already charge order.[13,16] Figure 3 also shows the resistivity of $Bi_{0.75}Sr_{0.25}MnO_3$ measured under field ($\mu_0 H=5$ T, heating), and confirms that this oxide does not present significant magnetoresistance, although the field deviates the resistivity slightly below the evolution of the ZF curve at low temperature. The small deviation of the resistivity under field was only observed in $Bi_{0.75}Sr_{0.25}MnO_3$, but does not take place, increasing the Sr content, in the perovskite with $x=0.50$. The onset of long range magnetic order below $T_N=120$ K does not produce changes in the thermal evolution of $\rho(T,H)$.

C. High magnetic field study

The temperature dependence of the magnetization (measured under 1 T, field cooled) and the inverse susceptibility of $Bi_{0.75}Sr_{0.25}MnO_3$ are depicted in Fig. 2(b). To be noticed is that the evolution of M(T) shows a ferromagnetic component below the magnetic transition at low temperature. We observe that ferromagnetic moment is, at 5 K, 0.78 μ_B/Mn ion (1 T). Of interest is thus the different M(T) evolution in the charge-ordered phase of composition $x=1/4$, with respect the charge-ordered phase of $x=1/2$ [Fig. 2(b)]. The half doped material remains globally antiferromagnetic (AFM) below $T_N(\approx 110$ K).[2] This is in contrast with the M(T) evolution in the underdoped $x=0.25$ specimen, which develops a ferromagnetic component. In addition, the moderate value of this component would indicate ferrimagnetism below $T_N \approx 120$ K. This behavior was already found in Ref. [23], and one of the motivations of the present study was to investigate the astonishing coexistence of ferromagnetism and charge or orbital order in our sample. At this point we recall that $BiMnO_3$ is ferromagnetic below $T_C=105$ K and the origin of ferromagnetism in pure $BiMnO_3$ is a long-standing open question.[25–28] The saturation moment found in the pure perovskite is 3.6 μ_B/Mn,[25] a value slightly lower than expected for a perfect alignment of Mn^{3+} moments (4 μ_B/Mn). In a series of pioneer studies[23,25] Chiba *et al.* prepared $Bi_{1-x}Sr_xMnO_3$ ceramic samples (using conventional and high-pressure synthesis techniques), with x ranging from 0 to 0.67. Figure 2(c) reproduces the ferromagnetic component reported by Chiba *et al.* in Ref. 23 as a function of the Sr content (obtained from magnetization measurements). Ignoring the existence of charge order in these compounds, they found that doping with Sr systematically decreases the ferromagnetic moment from the saturation value of 3.6 μ_B observed in the parent $BiMnO_3$ perovskite. Consequently, they concluded that a characteristic feature of the low-doped region of $Bi_{1-x}Sr_xMnO_3$ is the persistence of a ferromagnetic component, which only disappeared at doping levels $x>0.4$.[23] In this context, one of the objectives of the present study has been to investigate the origin and nature of ferromagnetism in $Bi_{1-x}Sr_xMnO_3$ at moderate doping.

High-magnetic-field magnetization of two $Bi_{1-x}Sr_xMnO_3$ samples, with $x=0.33$ and 0.50, was measured at the facilities of the LNCMP in Toulouse (France). We recall that the composition $x=0.33$ exhibits the same structural transition, modulation and charge-order phase than the compound with $x=0.25$.[13,14] Using the discharge of a bank capacitor in a coil, pulsed high magnetic fields are obtained with a duration time of 0.6 s. The isothermal magnetization measurements were done at 4.2 K after a zero-field cooling process. At this temperature, the field dependence magnetization of the modulated phase of $Bi_{0.67}Sr_{0.33}MnO_3$ is shown in Fig. 4(a) up to 30 T (up sweep). In the same figure the M-H curve is compared with the curve obtained for $Bi_{0.50}Sr_{0.50}MnO_3$ up to 48 T using the same setup. In addition, Fig. 4(b) displays the behavior of M(H) in $Bi_{0.75}Sr_{0.25}MnO_3$ during a hysteresis cycle at 5 K (up to 6 T). An interesting result is that, in contrast with the M(T) curve of Fig. 2(b) (measured under a field of 1 T) which suggests a net FM component, the evolution of M(H) at low fields evidences that the CO phase of $Bi_{0.75}Sr_{0.25}MnO_3$ and $Bi_{0.67}Sr_{0.33}MnO_3$ (as in $Bi_{0.50}Sr_{0.50}MnO_3$) is globally antiferromagnetic in zero field. The hysteresis cycle for our sample $x=0.25$ is shown in Fig. 4(b) ($M_0=0.067$ μ_B/Mn, $H_c=665$ Oe), and intrinsic spontaneous ferromagnetism was ruled out. To be emphasized is that the AFM ground state is an unexpected conclusion after the work of Chiba *et al.*,[23] which suggested spontaneous ferromagnetism. Nevertheless, it is interesting to note that there is a remarkable difference between compositions $x=0.25$ and 0.50 in Fig. 4. In contrast with the linear M-H evolution of $Bi_{0.50}Sr_{0.50}MnO_3$, the magnetization curves for $x=0.25$ and 0.33 samples show an apparent nonlinear increase. The marked curvature in the M(H) isotherms of the last two samples curves confirms the induction of ferromagnetism by the external field. The ferromagnetic component increasing continuously with the field. The M(H) curve of $Bi_{0.50}Sr_{0.50}MnO_3$ displays a quasilinear increase that precludes spontaneous or field induced ferromagnetism at low or moderate fields [the beginning of a field induced transition is visible only above ≈ 37 T (Ref. 29)]. Therefore, although we have confirmed the induction of ferromagnetic components in low fields, we did not observe spontaneous ferromagnetism in zero field. Coinciding with this magnetic measurement, we will show in the next section that neutron diffraction data provide the same conclusion. A continuous progressive canting of the moments seems to occur under external field in $Bi_{0.75}Sr_{0.25}MnO_3$. This effect is already visible even for very small fields ($\ll 1$ T). Moreover, it is worthwhile noticing that (i) there is no evidence of charge order

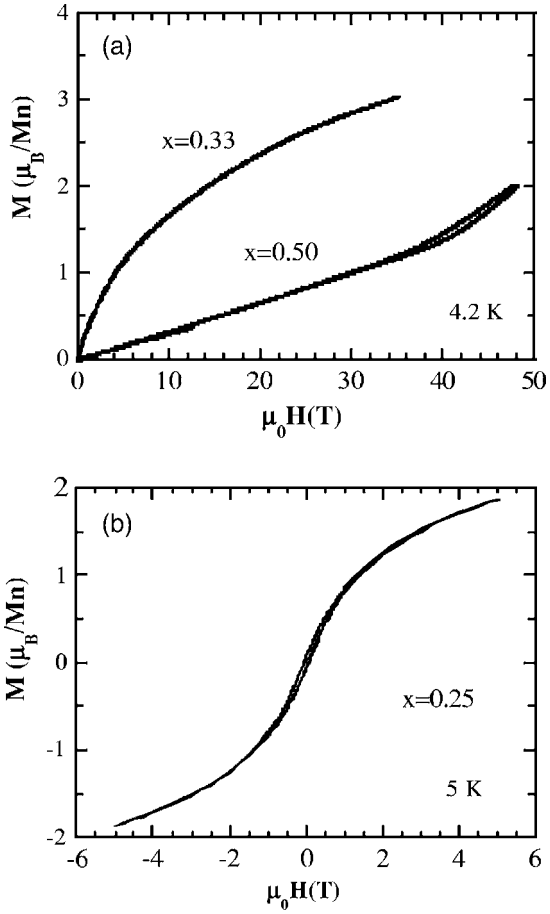

FIG. 4. (a) Magnetization vs field curves measured (at 4.2 K) in the charge-order phase of $Bi_{0.67}Sr_{0.33}MnO_3$ and $Bi_{0.50}Sr_{0.50}MnO_3$ (ZFC, pulsed high magnetic fields). Note that compounds with $x=0.33$ and 0.25 present the same modulated phase (Refs. 14 and 16). (b) M(H) of $Bi_{0.75}Sr_{0.25}MnO_3$ (ZFC, 5 K) obtained during a hysteresis cycle.

melting up to 30 T; and (ii) at this field the ferromagnetic moment is very close to 3 μ_B/Mn ion.

We bring to mind that the ferromagnetic ground state and the monoclinic $C2$ distortion of the pure oxide $BiMnO_3$ are related with the polarization of the Bi^{3+} lone-pair in the structure.[25] The persistence of ferromagnetism with increasing x in the magnetization of $Bi_{1-x}Sr_xMnO_3$ (found to vanish only $x>0.4$), was interpreted in Ref. 23 as a progressive dilution of the ferromagnetic ground state of $BiMnO_3$. Such a scenario would require the persistence of regions in the material retaining the peculiar monoclinic structure (space group $C2$) of $BiMnO_3$. We surveyed this possibility during the analysis of our ultrahigh resolution synchrotron data. Although we examined carefully our data, mesoscopic regions of $C2$ symmetry were neither detected in our high-resolution synchrotron and neutron measurements, nor in TEM data of the $x=0.25$ compound. Thereby, the possible presence of mesoscopic regions in the material having the structural symmetry of $BiMnO_3$ was ruled out. On the contrary, $Bi_{0.75}Sr_{0.25}MnO_3$ presents a new and well-crystallized charge modulation, very stable against temperature and compositional fluctuations. So, our current knowledge of this system

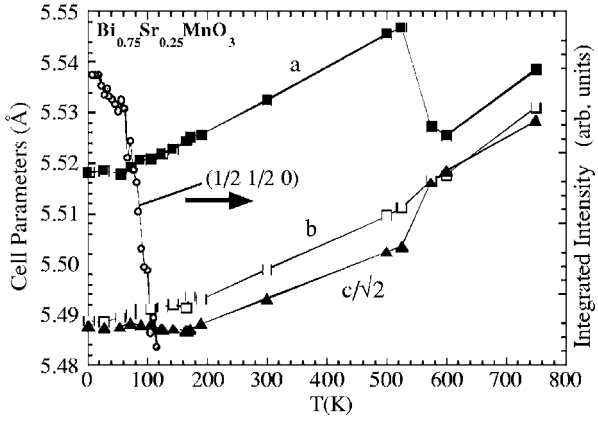

FIG. 5. Temperature dependence of the lattice parameters across the magnetic and electronic transitions (left axis). Integrated intensity of (1/2 1/2 0) magnetic peak in $Bi_{0.75}Sr_{0.25}MnO_3$ (from neutron data, right axis).

suggests a robust ordered phase, which cannot be seen as the result of a progressive disordered dilution of the $BiMnO_3$ structure by Sr substitution.

D. Neutron diffraction and magnetic structure

The structural study reported in Ref. 16 was based on diffraction data taken between RT and 750 K. In this section we present a neutron diffraction study of the magnetic order in the low temperature region. Neutron diffraction patterns were collected between 3 K and RT using D1B ($\lambda=2.52$ Å) and D2B ($\lambda=1.594$ Å) diffractometers. At 3 K the D2B diffractometer was used in high resolution mode. The evolution of the lattice parameters in the temperature interval 3–750 K is shown in Fig. 5. In the whole temperature range the sample behaved as a single phase, confirming the absence of phase segregation (unlike other compositions of the Bi—Sr phase diagram[9–11]). Coming from high temperatures the a axis rapidly increases as the sample undergoes charge ordering, while strikingly b and c decrease. The change in the a axis is the largest, and the drop of b is much smaller than the contraction of c. The lattice constant anomalies associated to T_{CO} look essentially complete at room temperature, far above T_N. Below room temperature, Fig. 5 shows the absence of clear anomalies at T_N. Given that the new superstructure is characterized by a modulation that doubles a and c lattice parameters (referred to the *Ibmm* subcell), we explored with special attention the possible existence of magnetic reflections (h k l) with h or l half integer. Coinciding with the low temperature anomaly in the magnetic susceptibility, we observed the appearance of a set of magnetic reflections below $T_N=120$ K. They were clearly visible at low temperatures in the low-angle region of the neutron diffraction patterns (Fig. 6). As an example, the evolution of the integrated intensity of the magnetic peak (1/2 1/2 0) is shown in Fig. 5.

Indexation of these magnetic peaks is possible on the basis of an orthorhombic $2ax2bxc$ magnetic cell (a,b,c referred to the average *Ibmm* cell, see Fig. 7). Magnetic peaks display (h k l) Miller indices with l integer and even, and h

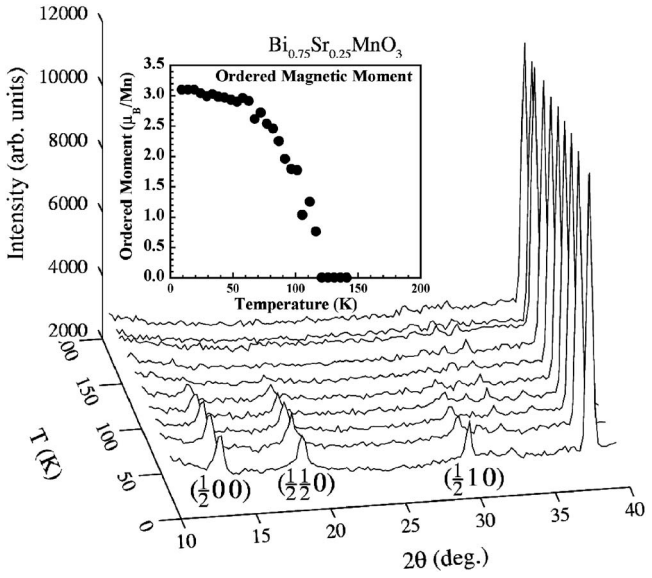

FIG. 6. Evolution in the temperature range 1.5–200 K of the low-angles portion of the neutron diffraction patterns showing the appearance of the main magnetic reflections ($\lambda = 2.52$ Å). The three most intense magnetic peaks are (1/2 0 0), (1/2 1/2 0), and (1/2 1 0). Inset: Evolution of the ordered magnetic moment determined from neutron data.

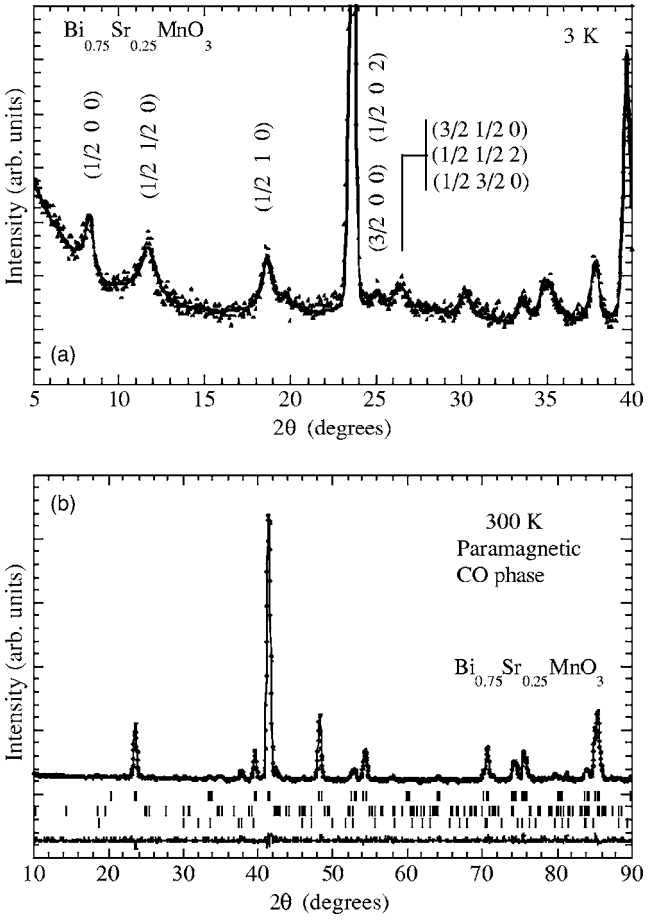

FIG. 7. (a) Low-angle region of the Rietveld refinement of the magnetic intensities from neutron powder diffraction at 3 K ($\lambda = 1.594$ Å). The structural contribution was fixed according to the structural model (*Ibmm*) detailed in Ref. 16 that reproduces the neutron and synchrotron data at RT. The goodness of the fit to the most conspicuous magnetic peaks is shown (magnetic peaks are labeled in the *Pbmn* setting). (b) Rietveld refinement of neutron data at 300 K (*Ibmm*), when the sample is paramagnetic. The second line of rows corresponds to the superstructure peaks [from the supercell, indexed as satellites of the mean *Ibmm* structure using wave vectors (1/2 0 0) and $(1/2\ 0\ \frac{1}{2})$, and reproduced using pattern matching], and the third line to Mn_3O_4 (1.5%).

or k or both half integer. The most conspicuous magnetic peaks correspond to indices (1/2 0 0), (1/2 1/2 0), (1/2 1 0), and with less intensity (3/2 0 0)/(1/2 0 2), (3/2 1/2 0), (1/2 1/2 2), and (1/2 3/2 0). In half doped CO manganites, magnetic peaks having l even are associated with the so-called pseudo-CE magnetic ordering.[29] In the opposing case, l is always odd in the canonical CE-type magnetic order.[1,3] The antiferromagnetic arrangement within the planes is identical for pseudo-CE and CE structures. However, while the antiferromagnetic Mn—O layers are ferromagnetically coupled along the c axis in the pseudo-CE magnetic structure (l even), this coupling is antiferromagnetic in the CE structures.[1,30] So, the absence of magnetic intensities with l odd rules out an antiferromagnetic coupling between adjacent a-b layers in the present case. With respect to half doped Bi—Sr, the perfect balance Mn^{4+}: $Mn^{3+}=1$ is altered by the extra e_g electrons in $Bi_{0.75}Sr_{0.25}MnO_3$. Half of the Mn^{4+} sites are in our case now occupied by the extra e_g electrons. We carried out a careful analysis of the diffracted magnetic intensities visible below 120 K using a number of magnetic models. We checked for different solutions, some involving (i) identical Mn moments and others involving (ii) two distinguishable manganese moments (Mn^{3+},Mn^{4+}). Finally, the best agreement between observed-calculated magnetic intensities was obtained with the same value of the magnetic moment in all Mn sites. The three best solutions found are gathered in Table I. All them correspond to pseudo-CE type magnetic arrangements: the only difference between models 1, 2, and 3 in Table I is the projection of the moments along the three main crystallographic axes. In model 3 the moments have been confined to the xy plane, as occurs in most of the charge-ordered manganites, without a magnetic component parallel to c. In model 2 moments are constrained to the xz plane. Finally, in model 1 the fits were performed without imposing limitations to the orientation of the moments in the pseudo-CE arrangement. The best agreement was obtained for Model 1 (see Tables I and II). A satisfactory fit of the magnetic intensities are obtained with an ordered moment $m(\mathrm{Mn}) = 3.10(6)\ \mu_B$ per Mn site, practically confined to the xz plane, but presenting a much smaller component parallel to the b axis (Fig. 7). Thus the best magnetic model corresponds to the projections: $m_x(\mathrm{Mn}) = 2.74\mu_B$, $m_y(\mathrm{Mn}) = 0.42\mu_B$, and $m_z(\mathrm{Mn}) = 1.35\mu_B$. It is necessary to underline the substantial improvement obtained on going from model 2 ($R_{MAG}=7.8\%$) to model 1 ($R_{MAG}=4.6\%$). This improvement strongly indicates the presence of a small magnetic component ($\sim 0.4\ \mu_B$) parallel to b. Consequently, we are led to conclude that the spin orientation presents no-null projections along the three direc-

TABLE I. Observed and calculated integrated intensities (3 K) for the main magnetic reflections. The magnetic components are referred to the *Ibmm* cell.

		Magnetic model 1		Magnetic model 2		Magnetic model 3	
		$m_X=2.74(6)\ \mu_B$ $m_Y=0.42(9)\ \mu_B$ $m_Z=1.35(4)\ \mu_B$ $\mathbf{m}[Mn]=3.10(6)\ \mu_B$		$m_X=2.54(4)\ \mu_B$ $m_Y=0\ \mu_B$ $m_Z=1.35(4)\ \mu_B$ $\mathbf{m}[Mn]=2.88(4)\ \mu_B$		$m_X=1.90(5)\ \mu_B$ $m_Y=-1.30(5)\ \mu_B$ $m_Z=0\ \mu_B$ $\mathbf{m}[Mn]=2.30(3)\ \mu_B$	
$(h\ k\ l)$	$Q^{-1}(Å^{-1})$	$I_{observed}$	$I_{calculated}$	$I_{observed}$	$I_{calculated}$	$I_{observed}$	$I_{calculated}$
(1/2 0 0)	0.572	153	153	147	137	144	125
(1/2 1/2 0)	0.808	320	328	325	366	329	368
(1/2 1 0)	1.276	174	176	173	177	170	131
(3/2 0 0) (1/2 0 2)	1.718	71	69	64	57	68	69
(3/2 1/2 0)	1.803	22	23	28	27	37	37
(1/2 1/2 2)	1.806	95	101	94	93	114	115
(1/2 3/2 0)	1.810	87	81	84	84	53	53
Reliability factors:							
R_{MAG}		4.63		7.78		10.6	
χ^2		2.29		2.34		2.64	

tions of the crystallographic cell. A schematic view of the magnetic ordering proposed for $Bi_{0.75}Sr_{0.25}MnO_3$ is shown in Fig. 8.

About the magnetic homogeneity in the sample, we call attention to the fact that A-cation sites are occupied by a distribution of 75% trivalent bismuth and 25% divalent Sr. It is reasonable to assume that intrinsic compositional fluctuations and strain fields due to differences in the atomic size can be a source of local defects in the long-range order electronic configuration. This could favor the presence of some kind of local magnetic disorder in the material. We would like to highlight the high value of the average ordered moment found per Mn site $[m(Mn)=3.09(6)\ \mu_B]$, which corroborates the quality of the sample investigated.

Obtaining a detailed picture, at atomic level, of the magnetic and electronic features of the (so far unique) charge-order phase detected in $Bi_{3/4}Sr_{1/4}MnO_3$ is one of the best opportunities to discern between different microscopic models proposed in CO manganites.[3–8,17–20] Moreover, it represents a good occasion to build a comprehensible description of defective but commensurate CO compositions with $x<4/8:1/8$, 2/8, or 3/8. In the charge-order model of static Zener polarons extended to the underdoped case ($x<0.50$) the coexistence of ZP units (formed by pairs of Mn, having intermediate valence $\sim+3.5$) and Mn^{3+} ions is envisaged. The electrons in excess (with respect to half doping) would localize by polaronic distortions giving rise to $Mn^{3+}O_6$ octahedra. From the susceptibility, the effective paramagnetic moment above T_{CO} agrees with a mixture of Mn^{3+} and Mn^{4+} moments in the ratio $(1-x)/x$ (μ_{eff}[theor]=4.62(4) versus μ_{eff}[exp]=4.68(4) μ_B/Mn). In the paramagnetic regime below T_{CO} ($T_N<T<T_{CO}$), the paramagnetic moment is in better agreement with the ZP model (coexistence of half of the Mn ions in Mn^{3+} ionic state ($S=2$), and the other half forming ZP (with $S=7/2$ per ZP); μ_{eff}[theor]=5.32(6) versus μ_{eff}[exp]=5.26(2) μ_B/Mn) than with the ionic CO picture (x Mn^{4+} and $(1-x)$ Mn^{3+} moments, μ_{eff}[theor]=4.62(4) μ_B/Mn).

A key issue is whether extra e_g electrons are distributed randomly or in an ordered manner. The particular superstructure and lattice deformation observed in $Bi_{0.75}Sr_{0.25}MnO_3$ suggest cooperative atomic displacements driven by a well-ordered arrangement of localized polaronic electronic states. A commensurate ordering of localized carriers is suggested by the doubly modulated superstructure (another example of doubly modulated manganite is $La_{7/8}Sr_{1/8}MnO_3$, which has

TABLE II. Magnetic structure refined from NPD data at low temperature. Sites are referred to the average $\sqrt{2}a_p\times\sqrt{2}a_p\times 2a_p$ cell.

Mn sites	$m_x(\mu_B)$	$m_y(\mu_B)$	$m_z(\mu_B)$
$(\frac{1}{2}\ 0\ 0)\ (0\ \frac{1}{2}\ 0)\ (\frac{1}{2}\ 1\ 0)\ (1\ -\frac{1}{2}\ 0)$ $(\frac{1}{2}\ 0\ \frac{1}{2})\ (0\ \frac{1}{2}\ \frac{1}{2})\ (\frac{1}{2}\ 1\ \frac{1}{2})\ (1\ -\frac{1}{2}\ \frac{1}{2})$	2.74(6)	0.42(9)	1.35(4)
$(-\frac{1}{2}\ 0\ 0)\ (0\ -\frac{1}{2}\ 0)\ (1\ \frac{1}{2}\ 0)\ (-\frac{1}{2}\ 1\ 0)$ $(-\frac{1}{2}\ 0\ \frac{1}{2})\ (0\ -\frac{1}{2}\ \frac{1}{2})\ (1\ \frac{1}{2}\ \frac{1}{2})\ (-\frac{1}{2}\ 1\ \frac{1}{2})$	−2.74(6)	−0.42(9)	−1.35(4)

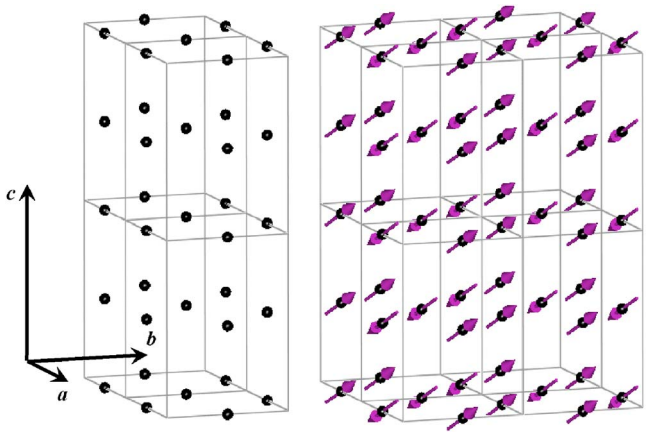

FIG. 8. (Color online). Schematic view of the magnetic structure of $Bi_{0.75}Sr_{0.25}MnO_3$ (as described in Table II). In the figure, the dimensions of the superstructure crystal cell (left) are compared with the magnetic cell.

in common with our $x=2/8$ sample the doubled periodicity along the *a* and *c* axis.[31–33] A more detailed picture of this orbital order structure requires single crystal neutron diffraction experiments, in order to solve completely the superstructure and identify the atomic displacements in the supercell. An arrangement of polaronic distortions is very likely in view of the unique features of this phase. Given the limited number of magnetic reflections detected in powder diffraction data, we cannot rule out a different magnetic arrangement, possibly derived from the "average" pseudo-CE magnetic structure. A variation of our description is not excluded if a much larger number of magnetic reflections were collected from a single crystal.

IV. CONCLUSION

In order to progress in the comprehension of the unique charge/orbital order phase of $Bi_{3/4}Sr_{1/4}MnO_3$, we have investigated the magnetic properties of this compound. The spectacular enhancement of the structural transition temperature (called CO transition) can probably be related with the high concentration of heavy Bi ions, having highly polarizable $6s^2$ electrons that can hybridize with O $2p$ states. After the pioneer studies of Chiba *et al.*[23] in this work we have studied the origin and nature of ferromagnetism in $Bi_{1-x}Sr_xMnO_3$ at moderate doping, and the possible coexistence of ferromagnetism and charge/orbital order in $Bi_{3/4}Sr_{1/4}MnO_3$. In contrast with other orbital ordered manganites with an excess of electrons (for moderate doping levels, $x \ll 0.50$), multiphase segregation tendencies were not observed in the present ordered phase. Microphase separation into ferromagnetic and antiferromagnetic regions was not detected and is unlikely in $Bi_{3/4}Sr_{1/4}MnO_3$. This oxide exhibits a well-crystallized modulation, very robust against temperature and compositional fluctuations.

The CO phase of $Bi_{0.75}Sr_{0.25}MnO_3$ presents long-range magnetic order below $T_N=120$ K. Above the magnetic transition, the Curie-Weiss behavior (120 K $< T <$ 575 K) exhibits positive $\theta_c=+104(2)$ K, indicative of dominant FM interactions. The effective paramagnetic moment found below T_{CO} [$\mu_{eff}=5.26(2)\ \mu_B$/Mn] disagrees with a coexistence of ionic Mn^{3+} and Mn^{4+} species (unlike what happens at $T > T_{CO}$). Conversely, the effective moment suggests the presence of charge localized states where the e_g electrons are shared by more than one Mn atom. The magnetic characterization confirms the results reported by Chiba *et al.*:[23] a net ferromagnetic moment at low temperature in the measurements performed under field under field ($M=0.8\ \mu_B$/Mn under $\mu_0 H=1$ T).

The periodicity of the magnetic structure determined from neutron powder diffraction differs from the dimensions of the superstructure cell (determined from electron, neutron, and x-rays synchrotron diffraction). Magnetic lines doubling the *c* (long) cell parameters were not detected in our study. The diffraction peaks with origin at the double periodicity along *c* are structural, they were present in the paramagnetic region below T_{CO} and do not vary across T_N. Our study reveals that previous interpretations, based on magnetic measurements under a field of $Bi_{1-x}Sr_xMnO_3$ ($0 < x < 0.5$) compounds, that suggested the occurrence of ferromagnetism, do not comply with the magnetic ground state in zero-field. The net ferromagnetic moment detected in previous works is not related to the persistence of the peculiar ferromagnetic structure of the pure $BiMnO_3$ phase. In zero field the magnetic structure is antiferromagnetic, ruling out the apparition of spontaneous ferromagnetism. However, the application of magnetic fields produces a continuous progressive canting of the moments, clearly visible even for relatively small fields ($H \ll 1$ T), but no appreciable changes in the resistivity (even at $\mu_0 H=5$ T). Application of high fields produces a remarkable and reversible spin polarization (under 30 T, the ferromagnetic moment is $\sim 3\ \mu_B$/Mn), without any sign of charge or orbital order melting. The coexistence of ferromagnetism and charge order at low and very high fields is a remarkable property of this system. The low temperature NPD patterns can be refined assuming a pseudo-CE antiferromagnetic (AFM) structure. It is interesting to observe that the orientation of the magnetic moments differs from previously reported "pseudo-CE" structures. Here, the magnetic moments are not confined within a crystallographic plane, and we have shown that finite magnetic components along the three perpendicular axes are required to reproduce the experimental magnetic intensities. Referred to the average *Ibmm* cell, ordered moments in the AFM collinear structure align according to $\mathbf{m}=[m_x=2.74(6), m_y=0.42(9), m_z=1.35(4)]\ \mu_B$ (Fig. 8). Consequently, the strongest component extends along the *a* direction, coinciding with the cell axis that experiences a substantial expansion below T_{CO} (*b* and *c* suffer a compression on cooling across T_{CO}). These results point towards a substantial proportion of Mn sites with e_g electronic density parallel to *a* axis in a orbital ordered phase.

ACKNOWLEDGMENTS

The collaboration and helpful discussions with M. Hervieu and A. Calleja is acknowledged. Financial support by the MEC (MAT2003-07483-C02-02) and Generalitat de

Catalunya (GRQ95-8029, PICS2005-14) is thanked. C.F. acknowledges financial support from MEC (Spain). We thank ILL, the CRG-D1B, and ESRF for the provision of beam time. The LNCMP in Toulouse is also acknowledged.

[1] E. O. Wollan and W. C. Koehler, Phys. Rev. **100**, 545 (1955).
[2] C. H. Chen and S.-W. Cheong, Phys. Rev. Lett. **76**, 4042 (1996).
[3] P. G. Radaelli, D. E. Cox, M. Marezio, and S.-W. Cheong, Phys. Rev. B **55**, 3015 (1997).
[4] S. Mori, C. H. Chen, and S.-W. Cheong, Nature (London) **392**, 473 (1998).
[5] M. Hervieu, A. Barnabé, C. Martin, A. Maignan, F. Damay, and B. Raveau, Eur. Phys. J. B **8**, 31 (1999).
[6] M. T. Fernández-Díaz, J. L. Martínez, J. M. Alonso, and E. Herrero, Phys. Rev. B **59**, 1277 (1999).
[7] P. G. Radaelli, D. E. Cox, L. Capogna, S.-W. Cheong, and M. Marezio, Phys. Rev. B **59**, 14440 (1999).
[8] A. Daoud-Aladine, J. Rodríguez-Carvajal, L. Pinsard-Gaudart, M. T. Fernández-Díaz, and A. Revcolevschi, Phys. Rev. Lett. **89**, 097205 (2002).
[9] C. Frontera, J. L. García-Muñoz, A. Llobet, C. Ritter, J. A. Alsonso, and J. Rodríguez-Carvajal, Phys. Rev. B **62**, 3002 (2000).
[10] J. L. García-Muñoz, C. Frontera, M. A. G. Aranda, A. Llobet, and C. Ritter, Phys. Rev. B **63**, 064415 (2001).
[11] M. Hervieu, A. Maignan, C. Martin, N. Nguyen, and B. Raveau, Chem. Mater. **13**, 1356 (2001).
[12] P. Beran, S. Malo, C. Martin, A. Maignan, M. Nevrîva, M. Hervieu, and B. Raveau, Solid State Sci. **4**, 917 (2002).
[13] C. Frontera, J. L. García-Muñoz, C. Ritter, L. Mañosa, X. Capdevila, and A. Calleja, Solid State Commun. **125**, 277 (2003).
[14] M. Hervieu, S. Malo, O. Perez, P. Beran, C. Martin, and B. Raveau, Chem. Mater. **15**, 523 (2003).
[15] J. L. García-Muñoz, C. Frontera, M. A. G. Aranda, C. Ritter, A. Llobet, M. Respaud, M. Goiran, H. Rakoto, O. Masson, J. Vanacken, and J. M. Broto, J. Solid State Chem. **171**, 84 (2003).
[16] C. Frontera, J. L. García-Muñoz, M. A. G. Aranda, M. Hervieu, C. Ritter, Ll. Mañosa, X. G. Capdevila, and A. Calleja, Phys. Rev. B **68**, 134408 (2003).
[17] R. J. Goff and J. P. Attfield, Phys. Rev. B **70**, 140404(R) (2004).
[18] S.Larochelle, A.Mehta, N.Kaneko, K. Mang, A. F. Panchula, L. Zhou, J. Arthur, and M. Grevenet, Phys. Rev. Lett. **87**, 095502 (2001).
[19] T. Nagai, T. Kimura, A. Yamazaki, Y. Tomioka, K. Kimoto, Y. Tokura, and Y. Matsui, Phys. Rev. B **68**, 092405 (2003).
[20] L. Brey, Phys. Rev. Lett. **92**, 127202 (2004).
[21] A. Calleja, X. Casas, I. Serradilla, M. Segarra, A. Sin, P. Odier, and F. Espiell, Physica C **372**, 1115 (2002).
[22] J. Rodríguez-Carvajal, Physica B **192**, 55 (1993).
[23] H. Chiba, T. Atou, and Y. Syono, J. Solid State Chem. **132**, 139 (1997).
[24] P. Beran *et al.* (unpublished).
[25] T. Atou, H. Chiba, K. Ohoyama, Y. Yamaguchi, and Y. Syono, J. Solid State Chem. **145**, 639 (1999).
[26] N. A. Hill and K. M. Rabe, Phys. Rev. B **59**, 8759 (1999).
[27] A. M. dos Santos *et al.*, Solid State Commun. **122**, 49 (2002).
[28] R. Seshadri and N. A. Hill, Chem. Mater. **13**, 2892 (2001).
[29] A. Kirste, M. Goiran, M. Respaud, J. Vanaken, J. M. Broto, H. Rakoto, M. von Ortenberg, C. Frontera, and J. L. García-Muñoz, Phys. Rev. B **67**, 134413 (2003).
[30] Z. Jirák, J. Hejtmánek, K. Knížek, M. Maryško, E. Pollert, M. Dlouhá, S. Vratislav, R. Kužel, and M. Hervieu, J. Magn. Magn. Mater. **250**, 275 (2002).
[31] Y. Yamada, O. Hino, S. Nohdo, R. Kanao, T. Inami, and S. Katano, Phys. Rev. Lett. **77**, 904 (1996).
[32] D. E. Cox, T. Iglesias, E. Moshopoulou, K. Hirota, K. Takahashi, and Y. Endoh, Phys. Rev. B **64**, 024431 (2001).
[33] T. Asaka, S. Yamada, S. Tsutsumi, C. Tsuruta, K. Kimoto, T. Arima, and Y. Matsui, Phys. Rev. Lett. **88**, 097201 (2002).